



<b>Title</b>	Interplay between the Beale-Kato-Majda theorem and the analyticity-strip method to investigate numerically the incompressible Euler singularity problem
<b>Authors(s)</b>	Bustamante, Miguel, Brachet, Marc E.
<b>Publication date</b>	2012-12-05
<b>Publication information</b>	Bustamante, Miguel, and Marc E. Brachet. "Interplay between the Beale-Kato-Majda Theorem and the Analyticity-Strip Method to Investigate Numerically the Incompressible Euler Singularity Problem" 86, no. 6 (December 5, 2012).
<b>Publisher</b>	American Physical Society
<b>Item record/more information</b>	<a href="http://hdl.handle.net/10197/7507">http://hdl.handle.net/10197/7507</a>
<b>Publisher's version (DOI)</b>	10.1103/PhysRevE.86.066302

Downloaded 2023-10-06T13:54:56Z

The UCD community has made this article openly available. Please share how this access benefits you. Your story matters! (@ucd\_oa)



© Some rights reserved. For more information

# Interplay between the Beale-Kato-Majda theorem and the analyticity-strip method to investigate numerically the incompressible Euler singularity problem

Miguel D. Bustamante

*School of Mathematical Sciences, University College Dublin, Belfield, Dublin 4, Ireland*

Marc Brachet

*Laboratoire de Physique Statistique, l'Ecole Normale Supérieure, F-75230 Paris Cedex 05, France and Associé au Centre National de la Recherche Scientifique et aux Universités Paris VI et VII, 24 Rue Lhomond, 75231 Paris, France*

(Received 7 December 2011; revised manuscript received 23 July 2012; published xxxxx)

Numerical simulations of the incompressible Euler equations are performed using the Taylor-Green vortex initial conditions and resolutions up to  $4096^3$ . The results are analyzed in terms of the classical analyticity-strip method and Beale, Kato, and Majda (BKM) theorem. A well-resolved acceleration of the time decay of the width of the analyticity strip  $\delta(t)$  is observed at the highest resolution for  $3.7 < t < 3.85$  while preliminary three-dimensional visualizations show the collision of vortex sheets. The BKM criterion on the power-law growth of the supremum of the vorticity, applied on the same time interval, is not inconsistent with the occurrence of a singularity around  $t \simeq 4$ . These findings lead us to investigate how fast the analyticity-strip width needs to decrease to zero in order to sustain a finite-time singularity consistent with the BKM theorem. A simple bound of the supremum norm of vorticity in terms of the energy spectrum is introduced and used to combine the BKM theorem with the analyticity-strip method. It is shown that a finite-time blowup can exist only if  $\delta(t)$  vanishes sufficiently fast at the singularity time. In particular, if a power law is assumed for  $\delta(t)$  then its exponent must be greater than some critical value, thus providing a new test that is applied to our  $4096^3$  Taylor-Green numerical simulation. Our main conclusion is that the numerical results are not inconsistent with a singularity but that higher-resolution studies are needed to extend the time interval on which a well-resolved power-law behavior of  $\delta(t)$  takes place and check whether the new regime is genuine and not simply a crossover to a faster exponential decay.

DOI: [10.1103/PhysRevE.00.006300](https://doi.org/10.1103/PhysRevE.00.006300)

PACS number(s): 47.10.-g, 47.11.Kb, 47.15.ki

## I. INTRODUCTION

A central open question in classical fluid dynamics is whether the incompressible three-dimensional Euler equations with smooth initial conditions develop a singularity after a finite time. A key result was established in the late 1980s by Beale, Kato, and Majda (BKM). The BKM theorem [1] states that blowup (if it takes place) requires the time integral of the supremum of the vorticity to become infinite (see the review by Bardos and Titi [2]). Many studies have been performed using the BKM result to monitor the growth of the vorticity supremum in numerical simulations in order to conclude yes or no regarding the question of whether a finite-time singularity might develop. The answer is somewhat mixed; see, e.g., [3–5] and the recent review by Gibbon [6]. Other conditional theoretical results, going beyond the BKM theorem, were obtained in a pioneering paper by Constantin, Fefferman, and Majda [7]. They showed that the evolution of the direction of vorticity posed geometric constraints on potentially singular solutions for the three-dimensional (3D) Euler equation [7]. This point of view was further developed by Deng, Hou, and Yu in [8] and [9].

An alternative way to extract insights on the singularity problem from numerical simulations is the so-called analyticity-strip method [10]. In this method the time is considered as a real variable and the space coordinates are considered as complex variables. The so-called width of the analyticity strip  $\delta(\geq 0)$  is defined as the imaginary part of the complex-space singularity of the velocity field nearest

to the real space. The idea is to monitor  $\delta(t)$  as a function of time  $t$ . This method uses the rigorous result [11] that a real-space singularity of the Euler equations occurring at time  $T_*$  must be preceded by a nonzero  $\delta(t)$  that vanishes at  $T_*$ . Using spectral methods [12],  $\delta(t)$  is obtained directly from the high-wave-number exponential falloff of the spatial Fourier transform of the solution [13]. This method effectively provides a “distance to the singularity” given by  $\delta(t)$  [14], which cannot be obtained from the general BKM theorem.

Note that the BKM theorem is more robust than the analyticity-strip method in the sense that it applies to velocity fields that do not need to be analytic. However, in the present paper we will concentrate on initial conditions that are analytic. In this case, there is a well-known result that states the following: “In three dimensions with periodic boundary conditions and analytic initial conditions, analyticity is preserved as long as the velocity is continuously differentiable ( $C^1$ ) in the real domain” [11]. The BKM theorem allows for a strengthening of this result: analyticity is actually preserved as long as the vorticity is finite [14].

The analyticity-strip method has been applied to probe the Euler singularity problem using standard periodic (and analytical) initial data: the so-called Taylor-Green (TG) vortex [15]. We now give a short review of what is already known about the TG dynamics. Numerical simulations of the TG flow were performed with resolution increasing over the years, as more computing power became available. It was found that, except for very short times and for as long as  $\delta(t)$  can be reliably measured, it displays almost perfect exponential

84 decrease. Simulations performed in 1982 on a grid of  $256^3$   
 85 points obtained  $\delta(t) \sim 2.60 e^{-t/0.57}$  (for  $t$  up to 2.5) [16]. This  
 86 behavior was confirmed in 1992 at resolution  $864^3$  [17]. More  
 87 than 20 years after the first study, simulations performed on  
 88 a grid of  $2048^3$  points yielded  $\delta(t) \sim 2.70 e^{-t/0.56}$  (for  $t$  up to  
 89 3.7) [18]. If these results could be safely extrapolated to later  
 90 times then the Taylor-Green vortex would never develop a real  
 91 singularity [13].

92 The present paper has two main goals. One is to report  
 93 on and analyze new simulations of the TG vortex that are  
 94 performed at resolution  $4096^3$ . These new simulations show a  
 95 well-resolved change of regime, leading to a faster decay of  
 96  $\delta(t)$  happening at a time where preliminary 3D visualizations  
 97 show the collision of vortex sheets.<sup>1</sup> The second goal of this  
 98 paper is to answer the following question, motivated by the new  
 99 behavior of the TG vortex: how fast does the analyticity-strip  
 100 width have to decrease to zero in order to sustain a finite-  
 101 time singularity, consistent with the BKM theorem? To the  
 102 best of our knowledge, this question has not been formulated  
 103 previously.

104 To answer this question we introduce a new bound of the  
 105 supremum norm of vorticity in terms of the energy spectrum.  
 106 We then use this bound to combine the BKM theorem with  
 107 the analyticity-strip method. This new bound is sharper than  
 108 usual bounds. We show that a finite-time blowup exists only if  
 109 the analyticity-strip width goes to zero sufficiently fast at the  
 110 singularity time. If a power-law behavior is assumed for  $\delta(t)$   
 111 then its exponent must be greater than some critical value. In  
 112 other words, we provide a powerful test that can potentially  
 113 rule out the existence of a finite-time singularity in a given  
 114 numerical solution of Euler equations. We apply this test to the  
 115 data from the latest  $4096^3$  Taylor-Green numerical simulation  
 116 in order to see if the change of behavior in  $\delta(t)$  can be consistent  
 117 with a singularity.

118 The paper is organized as follows: Sec. II is devoted to the  
 119 basic definitions, symmetries, and numerical method related  
 120 to the inviscid Taylor-Green vortex. In Sec. III, the new high-  
 121 resolution Taylor-Green results are presented and are analyzed  
 122 classically in terms of analyticity-strip method and BKM. In  
 123 Sec. IV, the analyticity-strip method and BKM theorem are  
 124 bridged together. The section starts with heuristic arguments  
 125 that are next formalized in a mathematical framework of  
 126 definitions, hypotheses, and theorems. In Sec. V, our new  
 127 theoretical results are used to analyze the behavior of the  
 128 decrement. Section VI is our conclusion.

129 The generalization to non-TG-symmetric periodic flows of  
 130 the results presented in Sec. IV is described in the Appendix.

## 131 II. DEFINITION OF THE SYSTEM

### 132 A. Basic definitions

133 Let us consider the 3D incompressible Euler equations for  
 134 the velocity field  $\mathbf{u}(x, y, z, t) \in \mathbb{R}^3$  defined for  $(x, y, z) \in \mathbb{R}^3$  and

in a time interval  $t \in [0, T)$ : 135

$$\frac{\partial \mathbf{u}}{\partial t} + \mathbf{u} \cdot \nabla \mathbf{u} = -\nabla p, \quad \nabla \cdot \mathbf{u} = 0. \quad (1) \quad 136$$

The Taylor-Green (TG) flow [15] is defined by the  $2\pi$ -  
 137 periodic initial data  $\mathbf{u}(x, y, z, 0) = \mathbf{u}^{\text{TG}}(x, y, z)$ , where 138

$$\mathbf{u}^{\text{TG}} = (\sin(x) \cos(y) \cos(z), -\cos(x) \sin(y) \cos(z), 0).$$

The periodicity of  $\mathbf{u}$  allows us to define the (standard)  
 139 Fourier representation: 140

$$\hat{\mathbf{u}}(\mathbf{k}, t) = \frac{1}{(2\pi)^3} \int_D \mathbf{u}(\mathbf{x}, t) \exp(-i\mathbf{k}\mathbf{x}) d^3x, \quad (2)$$

$$\mathbf{u}(\mathbf{x}, t) = \sum_{\mathbf{k} \in \mathbb{Z}^3} \hat{\mathbf{u}}(\mathbf{k}, t) \exp(i\mathbf{k}\mathbf{x}), \quad (3)$$

The kinetic-energy spectrum  $E(k, t)$  is defined as the sum  
 141 over spherical shells, 142

$$E(k, t) = \frac{1}{2} \sum_{\substack{\mathbf{k} \in \mathbb{Z}^3 \\ k-1/2 < |\mathbf{k}| < k+1/2}} |\hat{\mathbf{u}}(\mathbf{k}, t)|^2, \quad (4)$$

and the total energy, 143

$$E = \frac{1}{2(2\pi)^3} \int_D |\mathbf{u}(\mathbf{x}, t)|^2 d^3x = \frac{1}{2} \sum_{\mathbf{k} \in \mathbb{Z}^3} |\hat{\mathbf{u}}(\mathbf{k}, t)|^2,$$

is independent of time because  $\mathbf{u}$  satisfies the 3D Euler  
 144 equations (1). 145

### 146 B. Symmetries

A number of the symmetries of  $\mathbf{u}^{\text{TG}}$  are compatible with  
 147 the equation of motions. They are, first, rotational symmetries  
 148 of angle  $\pi$  around the axis ( $x = z = \pi/2$ ) and ( $x = z = \pi/2$ )  
 149 and of angle  $\pi/2$  around the axis ( $x = y = \pi/2$ ). A second  
 150 set of symmetries corresponds to planes of mirror symmetry:  
 151  $x = 0, \pi$ ,  $y = 0, \pi$ , and  $z = 0, \pi$ . On the symmetry planes, the  
 152 velocity  $\mathbf{u}^{\text{TG}}$  and the vorticity  $\omega^{\text{TG}} = \nabla \times \mathbf{u}^{\text{TG}}$  are, respec-  
 153 tively, parallel and perpendicular to these planes that form the  
 154 sides of the so-called impermeable box which confines the  
 155 flow. 156

It is demonstrated in [16] that these symmetries imply  
 157 that the Fourier expansion coefficients of the velocity field  
 158 in Eq. (3)  $\hat{\mathbf{u}}(m, n, p, t)$  vanish unless  $m, n, p$  are either all even  
 159 or all odd integers. This fact can be used in a standard way [16]  
 160 to reduce memory storage and speed up computations. 161

### 162 C. Numerical method

The Euler equations (1) are solved numerically using  
 163 standard [12] pseudospectral methods with resolution  $N$ . Time  
 164 marching is done with a second-order Runge-Kutta finite-  
 165 difference scheme. The solutions are dealiased by suppressing,  
 166 at each time step, the modes for which at least one wave-vector  
 167 component exceeds two-thirds of the maximum wave number  
 168  $N/2$  (thus a  $4096^3$  run is truncated at  $k > k_{\text{max}} \equiv 1365$ ). 169

The simulations reported in this paper were performed  
 170 using a special purpose symmetric parallel code developed  
 171 from that described in [19,20]. The workload for a time step  
 172 is (roughly) twice that of a general periodic code running at a  
 173 quarter of the resolution. Specifically, at a given computational  
 174

<sup>1</sup>This new behavior of the Euler TG vortex is somewhat similar to  
 the acceleration in the decrease of  $\delta$  that was reported in magnetohy-  
 drodynamics for the so-called IMTG initial data at resolution  $2048^3$   
 in [19].

175 cost, the ratio of the largest to the smallest scale available  
 176 to a computation with enforced Taylor-Green symmetries is  
 177 enhanced by a factor of 4 in linear resolution. This leads  
 178 to a factor of 32 savings in total computational time and  
 179 memory usage. The code is based on FFTW and a hybrid  
 180 message passing interface (MPI) OPENMP scheme derived  
 181 from that described in [21]. The runs were performed on the  
 182 Institut du Développement et des Ressources en Informatique  
 183 Scientifique BlueGene/P machine. At resolution  $4096^3$  we  
 184 used 512 MPI processes, each process spawning four OPENMP  
 185 threads.

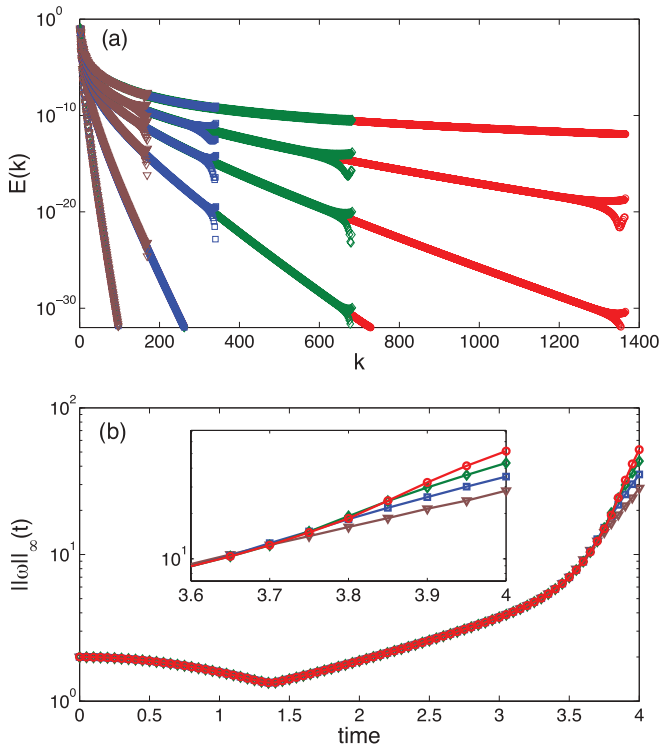
186 **III. NUMERICAL RESULTS AND CLASSICAL ANALYSIS**

187 **A. Energy spectra, maximum vorticity,**  
 188 **and collision of vortex sheets**

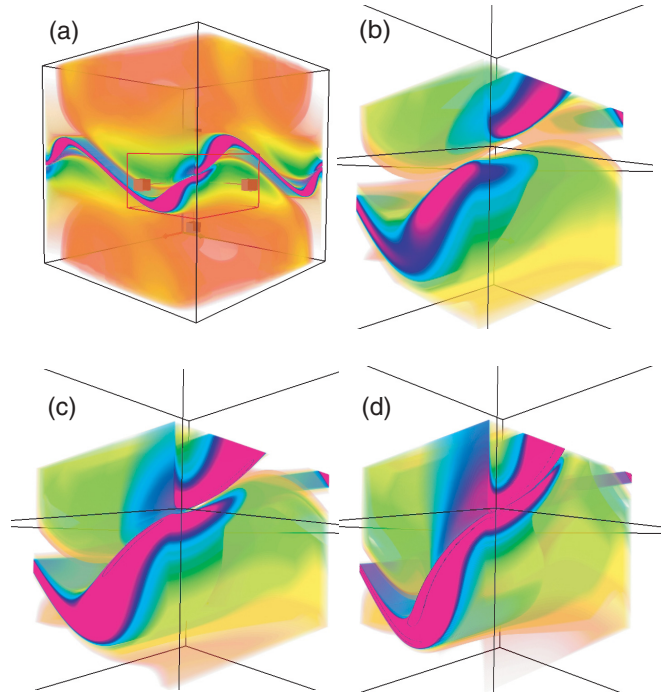
189 Runs were performed at resolutions  $512^3$ ,  $1024^3$ ,  $2048^3$ ,  
 190 and  $4096^3$ .

191 The behavior of the energy spectra in Eq. (4) and the  
 192 spatial maximum of the norm of the vorticity  $\omega = \nabla \times \mathbf{u}$  are  
 193 presented in Fig. 1.

194 It is apparent in Fig. 1(a) that resolution-dependent even-  
 195 odd oscillations are present, at certain times, on the TG energy  
 196 spectrum. Note that this behavior is produced when the tail  
 197 of the spectrum rises above the round-off error  $\sim 10^{-32}$ . This  
 198 phenomenon can be explained in terms of a *resonance* [22],



199 FIG. 1. (Color online) Temporal evolution of TG flow. (a) Energy  
 200 spectra  $E(k, t)$  [see Eq. (4)] at  $t = (1.3, 1.9, 2.5, 2.9, 3.4, 4.0)$ . The  
 201 lowest curve corresponds to  $t = 1.3$  and the highest corresponds  
 202 to  $t = 4.0$ . (b) Maximum of vorticity  $\|\omega(\cdot, t)\|_\infty$ . Results from runs  
 203 performed at different resolutions are displayed together:  $512^3$  (brown  
 204 triangles),  $1024^3$  (blue squares),  $2048^3$  (green diamonds), and  $4096^3$   
 205 (red circles).



206 FIG. 2. (Color online) 3D visualization of TG vorticity  $|\nabla \times \mathbf{u}|$  at  
 207 resolution  $4096^3$ . (a) Full impermeable box  $0 \leq x \leq \pi$ ,  $0 \leq y \leq \pi$ ,  
 208 and  $0 \leq z \leq \pi$  at  $t = 3.75$ . Zooms over the sub-box marked near  
 209  $x = y = \pi$ ,  $z = \pi/2$  are displayed at (b)  $t = 3.5$ , (c)  $t = 3.75$ , and  
 210 (d)  $t = 4.0$ .

211 along the lines developed in [23]. In practice we will deal with  
 212 this problem by averaging the spectrum over shells of width  
 213  $\Delta k = 2$ . Apart from this it can be seen that spectra computed  
 214 using different resolutions are in good agreement for all times.

215 In contrast, it is visible in Fig. 1(b) that the maximums of  
 216 vorticity  $\|\omega(\cdot, t)\|_\infty$  computed at different resolutions are in  
 217 agreement only up to some resolution-dependent time (see the inset).  
 218 The fact that  $\|\omega(\cdot, t)\|_\infty$  at a given time  $t > 3.7$  decreases  
 219 if one truncates the higher wave numbers of the velocity field  
 220 [see Fig. 1(b)] strongly suggests that  $\|\omega(\cdot, t)\|_\infty$  has significant  
 221 contributions coming from high-wave-number modes. This  
 222 forms the basis of the heuristic argument presented below in  
 223 Sec. IV A.

224 Figure 2 shows 3D visualizations (using the VAPOR<sup>2</sup>  
 225 software) of the high vorticity regions in the impermeable  
 226 box, corresponding to the  $4096^3$  run at late times. A thin vortex  
 227 sheet is apparent in Fig. 2(a) on the vertical faces  $x = 0, \pi$  and  
 228  $y = 0, \pi$  of the impermeable box.

229 The emergence of this thin vortex sheet is well understood  
 230 by simple dynamical arguments about the flow on the faces  
 231 of the impermeable box that were first given in [16]. We now  
 232 briefly review these arguments. The initial vortex on the bottom  
 233 face is forced by centrifugal action to spiral first outwards  
 234 toward the edges and then up the side faces. A corresponding  
 235 outflow on the top face and downflow from the top edges  
 236 onto the side faces lead to a convergence of fluid near the  
 237 horizontal centerline of each side face, from where it is forced

<sup>2</sup>See <http://www.vapor.ucar.edu>.

back into the center of the box and subsequently back to the top and bottom faces. The vorticity on the side faces is efficiently produced in the zone of convergence and builds up rapidly into a vortex sheet (see Figs. 1 and 2 of [16] and Fig. 8 of [17]).

While these considerations explain the presence of the thin vortex sheet in Fig. 2(a), the dynamics presented in Figs. 2(b)–2(d) also involves the collision of vortex sheets happening near the edge  $x = y = \pi$ , close to  $z = \pi/2$ . Note that, as stated above in Sec. II B, the vortex lines are perpendicular to the faces of the impermeable box. Thus, because the collision takes place near an edge, the corresponding vortex lines must be highly curved, with strong variations of the direction of vorticity. The geometric constraints on potential singularities posed by the evolution of the direction of vorticity developed in [7–9] could be applied to the situation described in Fig. 2. However, such an analysis goes beyond the BKM theorem and involves extensive postprocessing of very large datasets. This task is thus left for further work, and we concentrate here on simple BKM diagnostics for the vorticity supremum and analyticity-strip analysis of energy spectra.

### B. Analyticity-strip analysis of energy spectra

The analyticity-strip method [10] is based on the fact that when the velocity field is analytic in space the energy spectrum satisfies  $E(k, t) \propto e^{-2k\delta(t)}$  in the asymptotic “ultraviolet region”  $k \gg 1$ , with a proportionality factor that may contain an algebraic decay in  $k$ , a multiplicative function of time, and depending on the complexity of the physical flow, even an oscillatory (in  $k$ ) modulation [18].

The basic idea is thus to assume that  $E(k, t)$  can be well approximated by a function of the form

$$E(k, t) \approx C(t) k^{-n(t)} e^{-2k\delta(t)}$$

in some wave-number interval between 1 and  $k_{\max} = \lfloor N/3 \rfloor$  (the maximum wave number permitted by the numerical resolution  $N$ ). The common procedure to determine  $C(t), n(t), \delta(t)$  is to perform a least-square fit at each time  $t$  on the logarithm of the energy spectrum  $E(k, t)$ , using the functional form

$$\ln E(k, t) = \ln C(t) - n(t) \ln k - 2k\delta(t). \quad (5)$$

The error on the fit interval  $k_1 \leq k \leq k_2$ ,

$$\chi^2(t) = \sum_{k=k_1}^{k_2} [\ln E(k, t) - \ln C(t) + n(t) \ln k + 2k\delta(t)]^2,$$

is minimized by solving the equations  $\partial\chi^2/\partial C = 0$ ,  $\partial\chi^2/\partial n = 0$ , and  $\partial\chi^2/\partial\delta = 0$ . Note that these equations are linear in the parameters  $\ln C(t)$ ,  $n(t)$ , and  $\delta(t)$ .

The transient oscillations of the energy spectrum observed at the highest wave numbers [see Fig. 1(a)] are eliminated by averaging the TG spectrum on shells of width  $\Delta k = 2$  before performing the fit [16].

We present in Fig. 3 examples of TG energy spectra fitted in such a way on the intervals  $2 < k < \min(k^*, k_{\max})$ , where  $k^* = \inf_{E(k) < 10^{-32}}(k)$  denotes the beginning of round-off noise. It is apparent that the fits are globally of a good quality.

The time evolutions of the fit parameters  $C$ ,  $\delta$ , and  $n$  computed at different resolutions are displayed in Fig. 4. The measure of the fit parameters is reliable as long as  $\delta(t)$

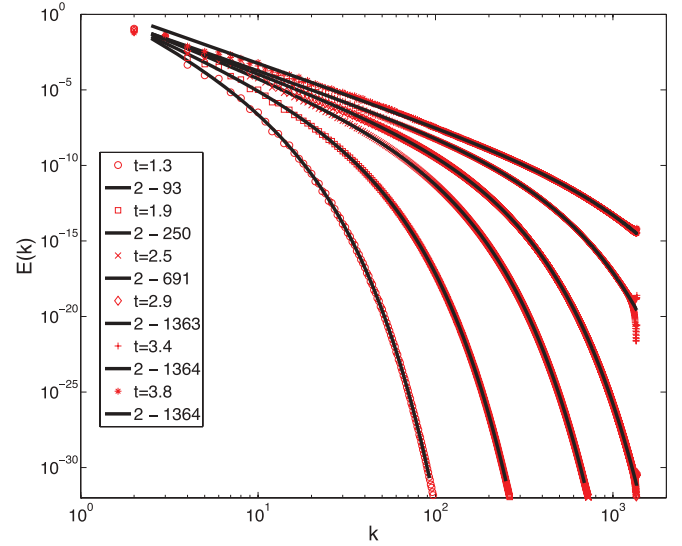


FIG. 3. (Color online) Comparison of fit in Eq. (5) (solid black line) and spectrum at resolution  $4096^3$  (red markers); times and fit intervals are indicated in the legend.

remains larger than a few mesh sizes, a condition required for the smallest scales to be accurately resolved and spectral convergence ensured. Thus the dimensionless quantity  $\delta k_{\max}$  is a measure of spectral convergence.

It is conventional [16] to define a “reliability time”  $T_{\text{rel}}$  by the condition

$$\delta(T_{\text{rel}})k_{\max} = 2 \quad (6)$$

and to say that the numerical simulation is reliable for times  $t \leq T_{\text{rel}}$ . This reliability time can be extended only by increasing the spatial resolution available for the simulation, so the more computer power is available the larger is the reliability time.

The resolution-dependent reliability condition Eq. (6) is marked by the horizontal lines in Fig. 4(c). The exponential law

$$\delta(t) \sim 2.70 e^{-t/0.56}, \quad (7)$$

that was previously reported at resolution  $2048^3$  in [18], is also indicated in Fig. 4(c) by a dashed black line. It is thus apparent that our lower-resolution results well reproduce the previous computations that were discussed above in Sec. I (see text preceding citation of [16–18]).

In Table I, the reliability time Eq. (6) obtained from the fit parameter  $\delta$  of Fig. 4 is compared with the reliability time stemming from the exponential behavior Eq. (7). It is apparent by inspection of the table that the reliability time of our new

TABLE I. Reliability time in Eq. (6) deduced from the exponential behavior in Eq. (7) compared with the reliability time obtained from the fit parameter  $\delta$  of Fig. 4.

Resolution	$T_{\text{rel}}$ (exponential law)	$T_{\text{rel}}$ (fit)
$512^3$	3.05	3.05
$1024^3$	3.43	3.44
$2048^3$	3.82	3.75
$4096^3$	4.21	3.85

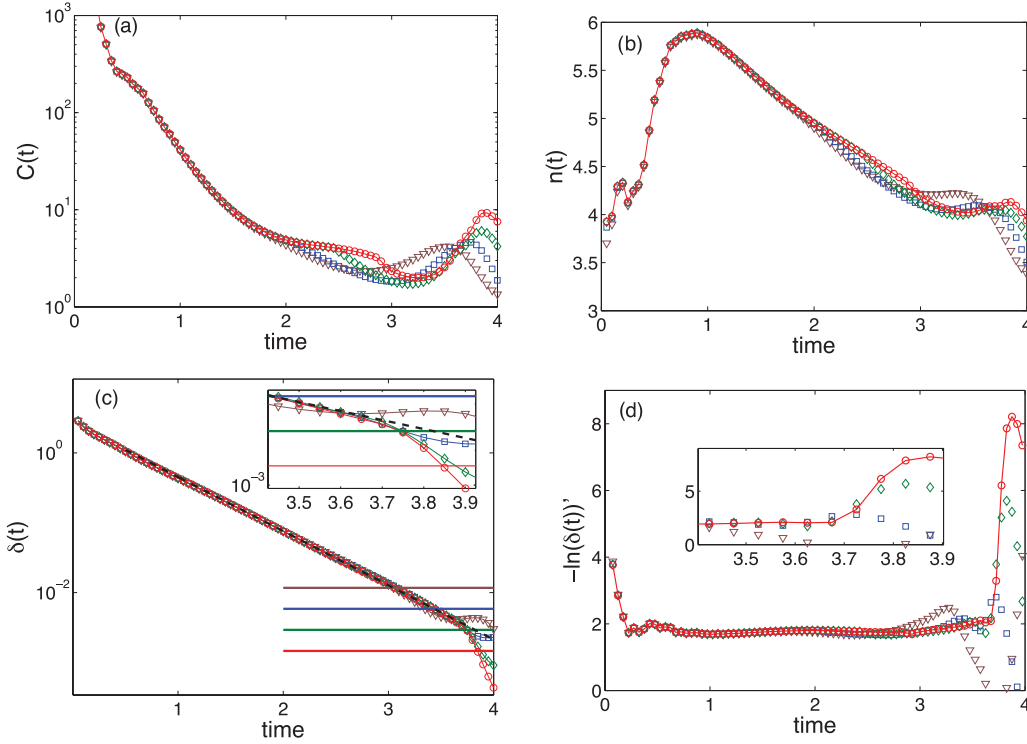


FIG. 4. (Color online) Time evolution of energy spectrum fit parameters [see Eq. (5) and Fig. 3]: (a) constant  $C$ , (b) prefactor  $n$ , (c) decrement  $\delta$  (horizontal lines,  $\delta k_{\max} = 2$ ; dashed black line, exponential law Eq. (7)), and (d) decay rate  $-d\{\ln[\delta(t)]\}/dt$ . Results corresponding to different resolutions are displayed together:  $512^3$  (brown triangles),  $1024^3$  (blue squares),  $2048^3$  (green diamonds), and  $4096^3$  (red circles).

298  $4096^3$  results is markedly smaller than that deduced from  
 299 the exponential law Eq. (7); the latter wrongly predicts that  
 300 simulations at this resolution should be reliable until  $t = 4.21$ .  
 301 The departure from the exponential behavior is also visible in  
 302 the inset in Fig. 4(c).

303 In order to capture this change of behavior more quan-  
 304 titatively the logarithmic decay rate  $-d \ln(\delta)/dt$ , computed  
 305 using finite differences in time, is displayed in Fig. 4(d). A  
 306 clear change in trend is apparent around  $t = 3.7$ , where the  
 307 logarithmic decay rate abruptly changes from a value near 2  
 308 to a value near 8. Note that this change of behavior happens  
 309 at a time that is reliable at resolution  $4096^3$  [see insets in  
 310 Figs. 4(c) and 4(d)]. Interestingly, this time is close to the  
 311 reliability time of the  $2048^3$  simulation. Therefore, the new  
 312 behavior of accelerated decay for times  $t > 3.7$  can only  
 313 be suggested by the  $2048^3$  data and is here demonstrated  
 314 by our  $4096^3$ -resolution data. This acceleration of the decay  
 315 rate of  $\delta(t)$  is important because if Eq. (7) could be safely  
 316 extrapolated to later times then the Taylor-Green vortex would  
 317 never develop a real singularity [13].

318 Let us conclude this section by showing that the new  
 319 behavior does not depend on the wave-number interval chosen  
 320 to perform the fits.

321 Indeed, by close inspection of the top curve in Fig. 3 one can  
 322 see that a small amount of systematic errors is present at the  
 323 lowest ( $k < 100$ ) wave numbers for large times. Excluding the  
 324 lowest wave numbers from the fits results in less errors (data  
 325 not shown). In Table II, the results of fits performed on the  
 326 subinterval  $103 < k < k_{\max}$  are compared with those on the  
 327 full interval  $3 < k < k_{\max}$  that was used until now. It can be  
 328 checked on the table that the departure from the exponential

law is not dependent on the interval chosen to perform the  
 fit. The values of  $n$  are also in agreement with previously  
 published data [18].

**C. BKM analysis of vorticity maximum**

In this section we look for eventual singular behavior  
 by focusing on the time dependence of the TG data for the  
 vorticity supremum  $\|\omega\|_{\infty}(t)$  that is displayed above in  
 Fig. 1(b). The BKM theorem [1] states that blowup (if it  
 takes place) requires the time integral of the supremum of  
 the vorticity to become infinite. Our analysis method, first  
 introduced in [5], looks at evidence of power-law behavior in  
 the numerical time series for  $\|\omega\|_{\infty}(t)$  to see if the computed  
 exponent is compatible with blowup of the time integral of  
 $\|\omega\|_{\infty}(t)$ . We now proceed to briefly recall the method.

TABLE II. Time evolution of fit parameters  $n$  and  $\delta$  [see Eq. (5)]  
 on full interval  $3 < k < k_{\max}$  (same as in Fig. 4) compared with fits  
 on subinterval  $103 < k < k_{\max}$ .

Time	$n$		$10^3 \times \delta$	
	$3 - k_{\max}$	$103 - k_{\max}$	$3 - k_{\max}$	$103 - k_{\max}$
3.6	4.07	3.95	4.13	4.22
3.65	4.09	4.05	3.73	3.75
3.7	4.09	4.14	3.36	3.31
3.75	4.09	4.19	2.85	2.76
3.8	4.12	4.29	2.10	1.95
3.85	4.13	4.34	1.41	1.22
3.9	4.09	4.34	0.94	0.71

343 Let  $f(t)$  be the quantity to be studied. In order to test if  
 344 it might blow up or go to zero in a finite time, we produce,  
 345 locally in time, fits of power-law behavior of the form

$$f(t) \approx c(T_* - t)^\gamma, \quad (8)$$

346 and we study the “instantaneous” or running estimates for  $\gamma$   
 347 and  $T_*$  as a function of time.

348 The local fits are done as follows: we first produce the new  
 349 function

$$g(t) = \left( \frac{d \ln f(t)}{dt} \right)^{-1} = f(t)/f'(t). \quad (9)$$

350 If  $f(t)$  is of the form of Eq. (8) then our new function satisfies  
 351  $g(t) \approx (T_* - t)/\gamma$ . Therefore, a linear fit of  $g(t)$  will give  $T_*$   
 352 and  $\gamma$ . More explicitly, we have the local expressions

$$\gamma(t) = \left( 1 - \frac{f(t) f''(t)}{f'(t)^2} \right)^{-1} \quad (10)$$

353 and

$$T_*(t) = t + \frac{f(t) f'(t)}{f(t) f''(t) - f'(t)^2}. \quad (11)$$

354 The latter local expressions can be used with any suitable fit  
 355 method of the data, not necessarily linear fits.

356 In practice, as our time series are given on an equally spaced  
 357 temporal grid, we proceed in the following straightforward  
 358 manner. First we compute  $\ln[f(t)]$ , then we use centered  
 359 finite differences to estimate its derivative. Inverting this data  
 360 furnishes estimates of  $g(t)$  at the midpoints. Using again  
 361 centered finite differences produces estimates of  $1/\gamma$  on the  
 362 original grid, thus allowing the determination of local estimates  
 363 for both  $T_*$  and  $\gamma$ . Note that this algorithm basically amounts  
 364 to a local three-point nonlinear fit.

365 The values of  $g(t)$ ,  $T_*(t)$ , and  $\gamma(t)$  obtained in this way from  
 366 the TG data for the vorticity supremum  $\|\omega\|_\infty$  are displayed  
 367 in Fig. 5. It is apparent that  $g(t)$  presents an inflection point  
 368 around  $t = 3.3$  corresponding to a maximum value of  $\gamma$  that is  
 369 above  $-1$ . Thus local in time power-law extrapolations around

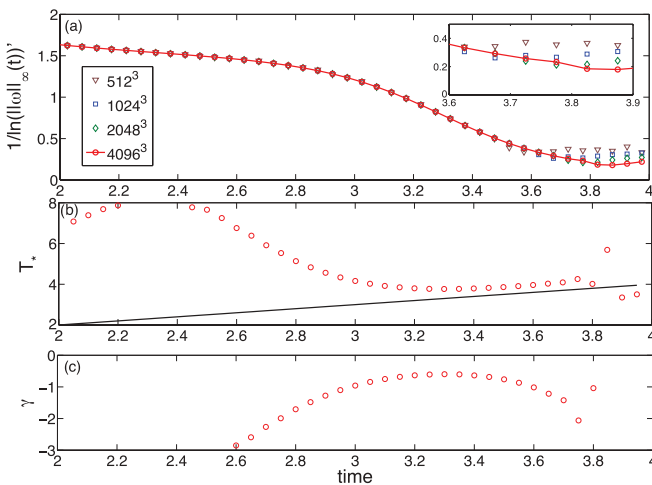


FIG. 5. (Color online) Time evolution of (a) inverse logarithmic derivative Eq. (9) at all resolutions (see legend), (b) extrapolated  $T_*$  (11) (solid black line:  $T_* = t$ ), and (c) running value of  $\gamma$  Eq. (10), both  $T_*$  and  $\gamma$  are shown only at resolution  $4096^3$  (red circles).

TABLE III. Power-law fit parameters  $\gamma$  and  $T_*$  [see Eq. (8)] for the vorticity supremum  $\|\omega\|_\infty$  determined at resolution  $4096^3$  [see Figs. 5(b) and 5(c)].

Time	$\gamma$	$T_*$
3.7	-1.42	4.09
3.75	-2.06	4.26
3.8	-1.04	4.02

$t = 3.3$  are inconsistent with the BKM theorem that requires  $\gamma \leq -1$ . However, when  $t$  is larger than 3.6, the value of  $\gamma$  goes below  $-1$  and thus becomes compatible with BKM.

On the other hand, there is no sign that the data values of  $\gamma$  and  $T_*$  are settling down into constants, corresponding to a simple power-law behavior.

Recall (see Sec. III B) that the last reliable value of  $\|\omega\|_\infty$  at resolution  $4096^3$  is at  $t = 3.85$ . Thus, due to our three-point extrapolation method, the last reliable data point is at  $t = 3.825$  in Fig. 5(a) and at  $t = 3.8$  in Figs. 5(b) and 5(c). The data corresponding to  $\gamma$  and  $T_*$  are also displayed in Table III.

Thus, our conclusion for this section is that although our late-time reliable data for  $\|\omega\|_\infty(t)$  show  $\gamma(t) < -1$  and are therefore not inconsistent with BKM, clear power-law behavior of  $\|\omega\|_\infty(t)$  is not achieved.

#### IV. BRIDGING ANALYTICITY-STRIP METHOD AND BKM THEOREM

##### A. Motivation and simple estimates

The vorticity maximum  $\|\omega(\cdot, t)\|_\infty$  was found to decrease when the resolution is reduced at any given time  $t > 3.7$  [see the above discussion following Fig. 1(b)]. This strongly suggests that, in this late-time regime,  $\|\omega(\cdot, t)\|_\infty$  has significant contributions coming from high-wave-number modes. In this context, the following short heuristic argument is provided as a motivation for the more rigorous mathematical results to follow.

Consider the well-known Sobolev inequality, which can be derived using the same hypotheses as in Lemma 7 below:

$$\|\omega(\cdot, t)\|_\infty \leq C_\epsilon \sqrt{2 \Omega_{\epsilon+5/2}(t)}, \quad \forall t \in [0, T]. \quad (12)$$

This bound is valid for any  $\epsilon > 0$ , where

$$C_\epsilon \equiv \sqrt{\sum_{\mathbf{k} \in \mathbb{Z}_{\text{odd}}^3 \cup \mathbb{Z}_{\text{even}}^3 \setminus \{0\}} |\mathbf{k}|^{-3-2\epsilon}}, \quad (13)$$

and  $\Omega_p$  is defined by

$$\Omega_p(t) \equiv \frac{1}{2} \sum_{\mathbf{k} \in \mathbb{Z}_{\text{odd}}^3 \cup \mathbb{Z}_{\text{even}}^3} |\mathbf{k}|^{2p} |\hat{\mathbf{u}}(\mathbf{k}, t)|^2. \quad (14)$$

Notice that  $2\Omega_p$  is the square of the Sobolev seminorm  $\|\mathbf{u}(\cdot, t)\|_{H^p}$ .

Motivated by the numerical results of Sec. III B, let us assume, at a given time  $t$ , a behavior of the energy spectrum in Eq. (4) of the type

$$E(k) \sim k^{-n} e^{-2\delta k}. \quad (15)$$

405 Notice that  $n$  and  $\delta$  are functions of time. When  $n < 6$  and  $\delta$   
 406 tends to zero, this gives a UV divergence:

$$\Omega_{\epsilon+5/2} \sim \int_1^\infty k^{5+2\epsilon-n} e^{-2\delta k} dk \sim \delta^{-6+n-2\epsilon}.$$

407 Plugging this into the bound Eq. (12), and using the BKM  
 408 theorem, we get  $\int_1^{T_*} \delta(t)^{-3+\frac{n}{2}-\epsilon} dt = \infty$ , where  $T_*$  is the  
 409 hypothetical singularity time.

410 At this point, again motivated by our numerical results, we  
 411 assume  $n = \text{const} < 6$  and assume a power-law behavior for  
 412 the analyticity-strip width of the form

$$\delta(t) \propto (T_* - t)^\Gamma,$$

413 where  $\Gamma > 0$  is a constant. Replacing this into the above  
 414 integral we conclude that

$$\int_1^{T_*} (T_* - t)^{(-3+\frac{n}{2}-\epsilon)\Gamma} dt = \infty,$$

415 i.e., a finite-time singularity can be attained only if the  
 416 exponents satisfy  $(-3 + \frac{n}{2} - \epsilon)\Gamma \leq -1$  for any  $\epsilon > 0$ . Taking  
 417 the limit  $\epsilon \rightarrow 0$  we deduce finally

$$\Gamma \geq \frac{2}{6-n}.$$

418 In words, “if the analyticity-strip width  $\delta(t)$  goes to zero as a  
 419 power law, then the exponent must be greater than or equal to  
 420  $\frac{2}{6-n}$ .”

421 The main difficulty to overcome in order to materialize  
 422 the above heuristic arguments into a firm basis is that the  
 423 common Sobolev bound Eq. (12) has a problem at  $\epsilon = 0$ :  
 424 the constant  $C_\epsilon$  is equal to infinity there, so taking the limit  
 425 as we did is not fully justified. We provide the solution to  
 426 this problem by finding a new rigorous bound, sharper than  
 427 the common Sobolev bound, which gives the same optimal  
 428 exponents without a divergent constant.

429 The second difficulty is that the assumed behavior for the  
 430 energy spectrum in Eq. (15), commonly used in the analyticity-  
 431 strip method, is a very strong condition and does not hold  
 432 uniformly for  $k \in \mathbb{N}$ . In fact, the evidence in analytically  
 433 solvable models such as the one-dimensional (1D) Burgers  
 434 equation is that the behavior Eq. (15) holds with some  
 435 exponents  $n$  and  $\delta$  in the region  $k \gg \delta^{-1}$ , (large- $k$  asymptotic  
 436 limit), and the behavior  $E(k, t) \sim k^{-\tilde{n}}$  holds in the region  
 437  $1 \leq k \ll \delta^{-1}$ , with  $\tilde{n} < n$ . We provide the solution to this lack  
 438 of uniformity by introducing a “working hypothesis” which is  
 439 a uniform-in- $k$  inequality for the energy spectrum, that still  
 440 retains the spirit of the analyticity-strip method. The working  
 441 hypothesis is verified for the case of the 1D Burgers equation  
 442 (see the discussion at the end of Sec. VI).

## B. Mathematical preliminaries

### 1. BKM theorem

445 We assume the usual hypotheses of the Beale-Kato-  
 446 Majda (BKM) theorem. Let  $T$  denote, from here on, a  
 447 generic time so that the velocity field  $\mathbf{u} \in C([0, T]; H^p) \cap$   
 448  $C^1([0, T]; H^{p-1})$ ,  $p \geq 3$ , so in particular the quantities defined  
 449 in Eq. (14) are bounded for  $p \geq 3$ :

$$\Omega_p(t) \leq c_p, \quad \forall t \in [0, T].$$

The BKM theorem [1] states that the assumed regularity of the  
 velocity field can be extended up to and including the time  $T$   
 if and only if  $\tau(T) \equiv \int_0^T \|\omega(\cdot, t)\|_\infty dt < \infty$ . By “regular up  
 to and including the time  $T$ ” we mean  $\mathbf{u} \in C([0, T]; H^p) \cap$   
 $C^1([0, T]; H^{p-1})$ ,  $p \geq 3$ .

*Definition 1.* We define the maximal time of regularity  
 $T_* \in (0, \infty]$  as the earliest time for which  $\mathbf{u}$  ceases to be in  
 $C([0, T]; H^p) \cap C^1([0, T]; H^{p-1})$ ,  $p \geq 3$ .

If  $T_* < \infty$  we speak of a finite-time singularity.

With this definition, we conclude that the time integral  
 appearing in the BKM theorem converges for all  $T < T_*$  and  
 diverges at  $T = T_*$ :  $\int_0^{T_*} \|\omega(\cdot, t)\|_\infty dt = \infty$ .

### 2. Working hypothesis for energy spectrum

An implicit assumption of the analyticity-strip method  
 is the existence of the Fourier components of the solution  
 of the 3D Euler equations. Taylor-Green (TG) symmetries  
 imply that only modes with even-even-even and odd-odd-odd  
 wave-number components are present (see Sec. II B). The  
 appropriate definition of the energy spectrum is thus the  
 following:

*Definition 2.* The kinetic-energy spectrum  $E(k, t)$  is defined  
 as the sum of the squares of the modulus of Fourier coefficients  
 over spherical shells:

$$E(k, t) = \frac{1}{2} \sum_{\substack{\mathbf{k} \in \mathbb{Z}^3 \\ \text{odd} \cup \text{even} \\ k-1/2 < |\mathbf{k}| < k+1/2}} |\hat{\mathbf{u}}(\mathbf{k}, t)|^2. \quad (16)$$

It is easy to check that the TG symmetries imply that  
 $E(0, t) = E(1, t) = 0 \quad \forall t \in [0, T_*)$ . Numerical observations  
 (see [18] and Sec. III above) lead us to formulate the following  
 working hypothesis that will be used to bound the energy  
 spectra:

*Hypothesis 3.* From here on, we will assume that there  
 exist a constant  $M > 0$  and positive functions  $n_0(t), \delta_0(t)$ ,  
 continuous on  $[0, T_*)$ , such that for all times  $t \in [0, T_*)$  and  
 all  $k \in \mathbb{Z}, k \geq 2$  we have

$$E(k, t) \leq M k^{-n_0(t)} e^{-2k \delta_0(t)}. \quad (17)$$

*Remarks.*

(i) The working hypothesis is consistent with the hypothe-  
 ses of the BKM theorem.

(ii) The working hypothesis is an inequality defined  
 globally in  $k$  and is not a large- $k$  asymptotic expansion.  
 Furthermore, a large- $k$  asymptotic expansion is typically of  
 the form  $E(k, t) = C_1(t) k^{-n_1(t)} e^{-2k \delta_1(t)}$  and has, in contrast  
 to Eq. (17), a time-dependent constant  $C_1(t)$ . Nevertheless,  
 asymptotic results can be used to establish the working  
 hypothesis in special cases such as the 1D inviscid Burgers  
 equation (see the discussion below, at the end of Sec. VI).

(iii) The numerically obtained fits of the analyticity-strip  
 method  $E(k, t) \approx C(t) k^{-n(t)} e^{-2k \delta(t)}$  are similarly related to the  
 working hypothesis. Notice that these fits are obtained over a  
 finite range of values of wave number  $k$ , so they give only  
 partial information. At early times, when the analyticity-strip  
 width  $\delta$  is big so that  $\delta k \gg 1$ , one is in the “large- $k$  asymptotic  
 limit.” At late times, when  $\delta$  becomes of the order of the highest  
 resolved wave number  $k_{\text{max}}$ , we have  $\delta k \lesssim 1$  and thus the



fits represent the “small- $k$  range.” The relations  $n(t) \geq n_0(t)$  and  $\delta(t) \geq \delta_0(t)$  are required for consistency with the working hypothesis. In practice, we will use the numerically obtained  $n(t)$  and  $\delta(t)$  to estimate  $n_0(t)$  and  $\delta_0(t)$ .

### 3. Classification of solutions in terms of regularity

We see from Definition 1 that a finite-time singularity is defined by the condition  $T_* < \infty$ . Combining this with the working hypothesis, a finite-time singularity can occur only if  $\lim_{t \rightarrow T_*} \delta_0(t) = 0$ . Among all possible continuous positive functions  $\delta_0(t)$  that tend to zero as  $t \rightarrow T_*$  we will consider, to simplify the analysis, only the power-law type of functions.

*Definition 4.* A solution of the 3D Euler equations satisfying the working hypothesis Eq. (17) is said to have a finite-time singularity of power-law type, with power  $\Gamma > 0$ , if the working hypothesis admits a function  $\delta_0(t)$  that behaves, near  $t = T_*$ , as

$$\delta_0(t) \propto (T_* - t)^\Gamma.$$

We saw in the heuristics Sec. IV A that if the energy spectrum is of the form  $E(k, t) \approx C(t)k^{-n(t)}e^{-2k\delta(t)}$  then the exponent  $n(t)$  must be less than 6 in order for a finite-time singularity to occur. This result will be fully formalized in Sec. IV C, but first we need to define two types of solutions in terms of the behavior of the exponent  $n_0(t)$  appearing in the working hypothesis.

*Definition 5.* A solution of the 3D Euler equations satisfying the working hypothesis Eq. (17) is said to be of strong regularity if the working hypothesis admits an exponent  $n_0(t)$  such that  $\liminf_{t \rightarrow T_*} n_0(t) > 6$ . Otherwise, i.e., if all the exponents admitted by the working hypothesis satisfy  $\liminf_{t \rightarrow T_*} n_0(t) \leq 6$ , the solution is said to be of mild regularity.

The reason for the name “strong” is due to the following lemma (to be proved in Sec. IV C):

*Lemma 6.* Let a solution of the 3D Euler equations satisfying the working hypothesis Eq. (17) be of strong regularity. Then the solution has no finite-time singularity.

This lemma’s assertion is basically the same as the well-known fact that there cannot be a finite-time loss of analytic regularity without loss of  $C^1$  regularity [11,24].

This result can be used as a validation test for numerical simulations of 3D Euler fluids. If the supremum norm of the vorticity is to grow in time without bound, then the exponent  $n_0(t)$  must be well below the critical value 6. Fortunately, all reliable numerical simulations that we know of pass this elementary test.

## C. Main results linking Beale-Kato-Majda theorem and analyticity-strip method

### 1. Sharp bound for vorticity

*Lemma 7.* Let  $\mathbf{u}(\mathbf{x}, t)$  be a velocity field satisfying the Taylor-Green symmetries and with energy spectrum defined by Eq. (16). Let  $\omega = \nabla \times \mathbf{u}$  be its vorticity, defined on the periodicity domain  $D = [0, 2\pi]^3$ . Then the following

inequality is verified for all times  $t \in [0, T)$ :

$$\|\omega(\cdot, t)\|_\infty \leq \sum_{k=2}^{\infty} \sqrt{2k(k+1)} E(k, t) S_k, \quad (18)$$

where  $S_k \equiv \#\{\mathbf{k} \in \mathbb{Z}_{\text{odd}}^3 \cup \mathbb{Z}_{\text{even}}^3 : k - 1/2 < |\mathbf{k}| < k + 1/2\}$  is the combined number of lattice points (of the form odd-odd-odd or even-even-even) in a spherical shell of width 1 and radius  $k \in \mathbb{Z}_+$ .

*Proof.* The vorticity field is defined in terms of its Fourier components by  $\omega(\mathbf{x}, t) = \sum_{\mathbf{k} \in \mathbb{Z}_{\text{odd}}^3 \cup \mathbb{Z}_{\text{even}}^3} e^{i\mathbf{k} \cdot \mathbf{x}} \widehat{\omega}(\mathbf{k}, t)$ . Therefore,

$$|\omega(\mathbf{x}, t)| \leq \sum_{\mathbf{k} \in \mathbb{Z}_{\text{odd}}^3 \cup \mathbb{Z}_{\text{even}}^3} |\widehat{\omega}(\mathbf{k}, t)|, \quad (19)$$

for all  $\mathbf{x} \in D$ . The left-hand side of this equation can be replaced by the supremum norm. Also, we use the identity  $|\widehat{\omega}(\mathbf{k}, t)| = |\mathbf{k}| |\widehat{\mathbf{u}}(\mathbf{k}, t)|$  on the right-hand side and obtain

$$\|\omega(\cdot, t)\|_\infty \leq \sum_{\mathbf{k} \in \mathbb{Z}_{\text{odd}}^3 \cup \mathbb{Z}_{\text{even}}^3} |\mathbf{k}| |\widehat{\mathbf{u}}(\mathbf{k}, t)|.$$

Assuming that  $\mathbf{u}$  is regular so the above sum over the lattice converges, we can rewrite the sum over spherical shells of width 1 and radius  $k \in \mathbb{Z}_+$ . We get

$$\|\omega(\cdot, t)\|_\infty \leq \sum_{k=2}^{\infty} \left( \sum_{\substack{\mathbf{k} \in \mathbb{Z}_{\text{odd}}^3 \cup \mathbb{Z}_{\text{even}}^3 \\ k-1/2 < |\mathbf{k}| < k+1/2}} |\mathbf{k}| |\widehat{\mathbf{u}}(\mathbf{k}, t)| \right).$$

We proceed to bound the terms in brackets, for a given  $k \in \mathbb{Z}_+$ . First, notice that the highest possible value of  $|\mathbf{k}|$  is equal to  $\sqrt{k(k+1)}$ . We obtain the preliminary result

$$\|\omega(\cdot, t)\|_\infty \leq \sum_{k=2}^{\infty} \sqrt{k(k+1)} \left( \sum_{\substack{\mathbf{k} \in \mathbb{Z}_{\text{odd}}^3 \cup \mathbb{Z}_{\text{even}}^3 \\ k-1/2 < |\mathbf{k}| < k+1/2}} |\widehat{\mathbf{u}}(\mathbf{k}, t)| \right).$$

Second, the remaining sum in brackets is related to the energy spectrum  $E(k, t)$ , Eq. (4), by virtue of the Cauchy-Schwartz inequality. We have

$$\sum_{\substack{\mathbf{k} \in \mathbb{Z}_{\text{odd}}^3 \cup \mathbb{Z}_{\text{even}}^3 \\ k-1/2 < |\mathbf{k}| < k+1/2}} |\widehat{\mathbf{u}}(\mathbf{k}, t)| \leq \sqrt{2E(k, t)} \sqrt{\sum_{\substack{\mathbf{k} \in \mathbb{Z}_{\text{odd}}^3 \cup \mathbb{Z}_{\text{even}}^3 \\ k-1/2 < |\mathbf{k}| < k+1/2}} 1}, \quad (20)$$

which establishes the lemma. ■

*Remarks.* The proof is independent of any evolution equation that  $\mathbf{u}$  might satisfy. Only two inequalities have been used to get the bound Eq. (18), and these inequalities are quite sharp:

First, the bound Eq. (19) is saturated when all phases are equal in the Fourier expansion for the vorticity field at the position of the vorticity maximum. This saturation indeed takes place in one-dimensional systems that blow up in a finite time, such as the inviscid Burgers equation (work in progress).

Second, the bound Eq. (20) is saturated when all the terms are equal in the sum over the spherical shell of fixed radius  $k$ . Physically, such saturation should be observed in a fully isotropic scenario, i.e., when the terms  $|\widehat{\mathbf{u}}(\mathbf{k}, t)|^2$  depend more on the wave vector’s modulus  $|\mathbf{k}|$  than on its direction  $\mathbf{k}/|\mathbf{k}|$ .

588 In contrast, the Sobolev bound Eq. (12) would be saturated  
 589 only for unphysical scenarios where the energy spectrum  
 590  $E(k, t)$  has a compact support in  $k$  space and is independent of  
 591 the wave number  $k$  on that support. Thus the Sobolev bound  
 592 Eq. (12) will be less sharp than the new bound Eq. (18) for any  
 593 realistic energy spectrum that decays as  $k \rightarrow \infty$ .

594 *Practical form.* We provide a more practical form of the  
 595 sharp bound Eq. (18), by noticing that  $S_k \approx \pi k^2$  as  $k \rightarrow \infty$ .  
 596 Under the hypotheses of Lemma 7, we readily obtain the  
 597 estimate

$$\|\omega(\cdot, t)\|_\infty \leq c \sum_{k=2}^\infty k^2 \sqrt{E(k, t)}, \quad (21)$$

598 where  $c = 2\sqrt{11/3}$ . This constant was computed by direct  
 599 inspection of the maximum deviation from the asymptotic  
 600 formula  $S_k \approx \pi k^2$ . Although this estimate seems not as sharp  
 601 as the original one, it will be enough for the practical situation  
 602 where the analyticity-strip width  $\delta(t)$  tends to zero and the  
 603 main contribution comes from the ‘‘ultraviolet region’’  $k \gg 1$ .

604 **2. Implications of BKM theorem: general result**

605 Let us replace the working hypothesis for the energy  
 606 spectrum Eq. (17) into the bound Eq. (21). The sum over  
 607  $k \geq 2$  can be written in terms of the so-called polylogarithm  
 608 function. We obtain the bound

$$\|\omega(\cdot, t)\|_\infty \leq c \sqrt{M} \tilde{\text{Li}}\left(\frac{n_0(t)}{2} - 2, e^{-\delta_0(t)}\right), \quad (22)$$

609 where  $\tilde{\text{Li}}(s, z)$  is defined by

$$\tilde{\text{Li}}(s, z) \equiv \sum_{k=2}^\infty k^{-s} z^k = \text{Li}(s, z) - z,$$

610 and  $\text{Li}(s, z)$  is the Jonquière’s function (or polylogarithm):  
 611  $\text{Li}(s, z) \equiv \sum_{k=1}^\infty k^{-s} z^k$ .

612 Combining the bound Eq. (22) with the BKM theorem we  
 613 obtain the following:

614 *Theorem 8.* Let a solution of the 3D Euler equations satisfy  
 615 the Taylor-Green symmetries and the working hypothesis  
 616 Eq. (17). Then its maximal regularity time  $T_*$  must satisfy

$$\int_0^{T_*} \tilde{\text{Li}}\left(\frac{n_0(t)}{2} - 2, e^{-\delta_0(t)}\right) dt = \infty. \quad (23)$$

618 *Proof.* The proof is a direct application of the BKM theorem  
 619 to inequality Eq. (22). ■

620 At this point it is necessary to state without proof some  
 621 properties of the polylogarithm:

622 *Lemma 9.* The polylogarithm function  $\text{Li}(p, z)$  satisfies the  
 623 following properties:

- 624 (i) Let  $0 < z < 1$  and let  $p, q$  be two non-negative numbers.  
 625 Then we have  $\text{Li}(p, z) \leq \text{Li}(q, z) \iff p \geq q$ .
- 626 (ii) Let  $|\mu| < 2\pi$  and let  $r \in \mathbb{R} \setminus \mathbb{Z}_+$ . Then  
 627

$$\text{Li}(r, e^\mu) \approx \Gamma(1 - r) (-\mu)^{r-1} + \sum_{k=0}^\infty \frac{\zeta(r - k)}{k!} \mu^k,$$

628 where  $\zeta$  is the Riemann zeta function.

(iii) Let  $|\mu| < 2\pi$  and let  $s \in \mathbb{Z}_+$ . Then

$$\text{Li}(s, e^\mu) \approx \frac{\mu^{s-1}}{(s-1)!} [H_{s-1} - \ln(-\mu)] + \sum_{\substack{k=0 \\ k \neq s-1}}^\infty \frac{\zeta(s-k)}{k!} \mu^k,$$

629 where  $H_p = \sum_{h=1}^p \frac{1}{h}$  is the  $p$ th harmonic number, with  
 630  $H_0 = 0$ .

631 We are now ready to prove the following:

632 *Lemma 6.* Let a solution of the 3D Euler equations satisfying  
 633 the working hypothesis Eq. (17) be of strong regularity. Then  
 634 the solution has no finite-time singularity.

635 *Proof.* By definition, solutions of strong regularity satisfy  
 636 the working hypothesis with  $\liminf_{t \rightarrow T_*} n_0(t) > 6$ .  
 637 Therefore, using Lemma 9 (i) on Eq. (23), we obtain  
 638  $\int^{T_*} \tilde{\text{Li}}(1 + \epsilon, e^{-\delta_0(t)}) dt = \infty$ , for some  $\epsilon \in (0, 1)$ . Now, using  
 639 Lemma 9 (ii) with  $r > 1$ , we obtain that the integrand is  
 640 continuous in time. Therefore  $T_* = \infty$ . ■

641 **3. Implications of BKM theorem: singularity scenarios**

642 Theorem 8 represents our ‘‘bridge’’ from the analyticity-  
 643 strip method to the BKM theorem: a singularity of the solution  
 644 at time  $T_*$  can be attained only if the parameters  $n_0(t)$  and  $\delta_0(t)$   
 645 satisfy Eq. (23).

646 Recall that for a singularity to occur the function  $\delta_0(t)$  must  
 647 tend to zero as  $t \rightarrow T_*$ . The polylogarithm  $\tilde{\text{Li}}(\frac{n_0(t)}{2} - 2, e^{-\delta_0(t)})$   
 648 has a branch point at  $n_0(t) = 6, \delta_0(t) = 0$  [see Lemma 9 (iii)],  
 649 so the asymptotic behavior of the integrand Eq. (23) as  $\delta_0(t) \rightarrow$   
 650 0 depends sensitively on the behavior of the function  $n_0(t)$  near  
 651 the ‘‘critical’’ value 6. To avoid this branch point, we introduced  
 652 solutions with strong and mild regularity in Definition 5.

653 The two following main results exploit the consequences  
 654 of Theorem 8 in singularity scenarios. They provide us with  
 655 a criterion on how fast  $\delta_0(t)$  must decay to zero in order to  
 656 sustain a singularity.

657 *Corollary 10.* Let a solution of the 3D Euler equations  
 658 satisfy the Taylor-Green symmetries and the working hy-  
 659 pothesis Eq. (17). Let the solution be of mild regularity, i.e.,  
 660  $\liminf_{t \rightarrow T_*} n_0(t) \leq 6$ , where  $T_*$  is the maximal regularity time.  
 661 Let  $\lim_{t \rightarrow T_*} \delta_0(t) = 0$ . Then,  $T_*$  satisfies

$$\int^{T_*} \left(\frac{1}{\delta_0(t)}\right)^{\frac{6-n_-}{2}} dt = \infty,$$

662 for all  $n_-$  in  $(-\infty, \liminf_{t \rightarrow T_*} n_0(t)] \cap (-\infty, 6)$ .

663 *Proof.* Let  $n_-$  be in  $(-\infty, \liminf_{t \rightarrow T_*} n_0(t)] \cap (-\infty, 6)$ .  
 664 From  $n_- \leq \liminf_{t \rightarrow T_*} n_0(t)$ , using Lemma 9 (i) on Eq. (23)  
 665 we obtain

$$\int^{T_*} \tilde{\text{Li}}\left(\frac{n_-}{2} - 2, e^{-\delta_0(t)}\right) dt = \infty.$$

666 Now, since  $n_- < 6$  and the function  $\delta_0(t)$  tends to zero as  
 667  $t \rightarrow T_*$ , we can use Lemma 9 (ii) to bound the integrand  
 668  $\tilde{\text{Li}}(\frac{n_-}{2} - 2, e^{-\delta_0(t)})$  by a constant times  $(\frac{1}{\delta_0(t)})^{\frac{6-n_-}{2}}$ , which com-  
 669 pletes the proof.

670 Finally we consider the hypothetical situation of a  
 671 finite-time singularity of power-law type, as described in  
 672 Definition 4:  $\delta_0(t) \propto (T_* - t)^\Gamma$ , with  $T_* < \infty$ .

673 *Corollary 11.* Under the hypotheses of Corollary 10, the  
 674 solution of the 3D Euler equations has a finite-time singularity  
 675

676 at time  $T_* < \infty$ , of power-law type with exponent  $\Gamma$ , only if

$$\Gamma \geq \frac{2}{6 - n_-},$$

677 for all  $n_-$  in  $(-\infty, \liminf_{t \rightarrow T_*} n_0(t)] \cap (-\infty, 6)$ .

678 *Proof.* The proof follows directly from Corollary 10. ■

679 **V. ANALYSIS OF ANALYTICITY-STRIP WIDTH**  
 680 **IN TERMS OF BKM THEOREM**

681 **A. Quality of bounds**

682 Several bounds were used in Sec. IV. We now proceed to  
 683 test their sharpness, when they are applied to the numerical data  
 684 of Sec. III. Figure 6 shows a comparison of the new inequality  
 685 Eq. (18) and the old inequality Eq. (12) taking  $\epsilon = 0.1$  with  
 686  $C_\epsilon = 3.9$ . Note that the value of  $C_\epsilon$  [see Eq. (13)] can be  
 687 estimated by the integral  $\sqrt{\int_{\sqrt{3}}^{\infty} \pi k^2 k^{-3-2\epsilon} dk} = \sqrt{\pi 3^{-\epsilon}/2\epsilon}$ ,  
 688 yielding  $C_\epsilon \sim 3.75$  at  $\epsilon = .1$ . A more careful computation of  
 689 the discrete sum gives  $C_\epsilon \gtrsim 3.9$ , the value used to generate  
 690 Fig. 6.

691 The data in Fig. 6(a) display two important facts:

692 (i) The new bound is sharper than the old bound throughout  
 693 the computation, particularly at the reliable end of the  
 694 simulation,  $t \gtrsim 3.7$ , when the three curves show a change of  
 695 trend and the old bound diverges at a faster rate than the  
 696 new bound [see also Fig. 6(b)].

697 (ii) Both old and new bounds are not too bad at the  
 698 beginning of the computation ( $t = 0$ ), with an initial ratio of  
 699 5:2 between the new bound and the vorticity supremum  
 700 norm. Subsequently, the bounds become increasingly less  
 701 sharp, and the new bound attains a ratio 165:1 with the  
 702 vorticity supremum norm at  $t = 4$ . However, the slope of

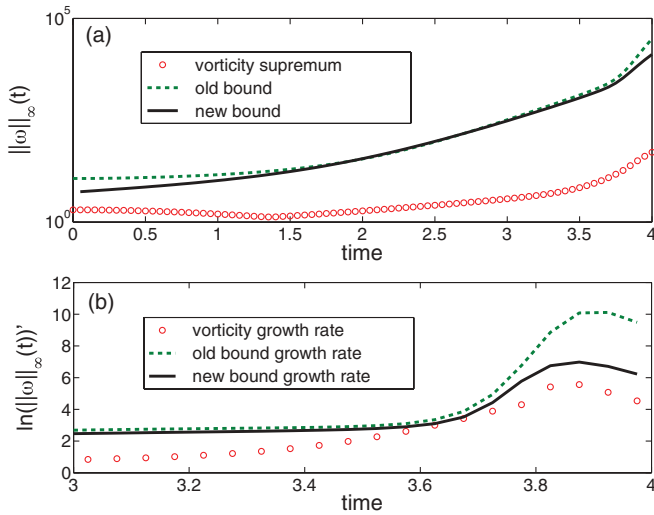


FIG. 6. (Color online) Comparison of the bounds for the Taylor-Green flow at resolution  $4096^3$ . (a) Lin-log plot: “old bound” is the right-hand side of the inequality Eq. (12), taking  $\epsilon = 0.1$  and  $C_\epsilon = 3.9$  (see text), and “new bound” is the right-hand side of the sharp inequality Eq. (18). (b) Interpolated time derivative of the logarithms of (a), for a time range localized near the change of trend, with the same parameters as in (a).

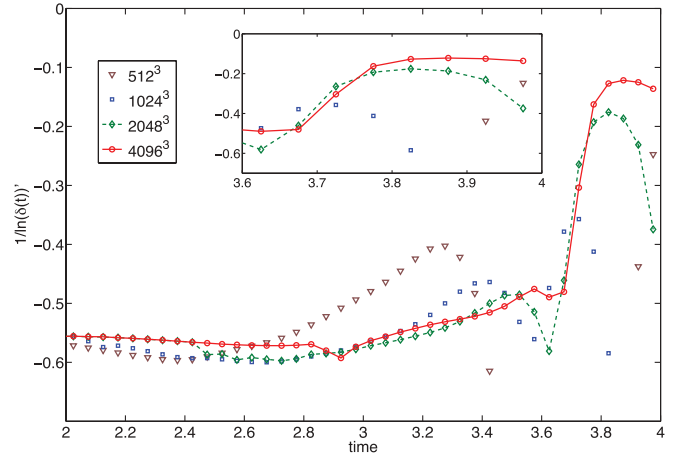


FIG. 7. (Color online) Temporal evolution of the inverse logarithmic derivative Eq. (9) computed from the same values of  $\delta$  as in Fig. 4(d);  $512^3$  (brown triangles),  $1024^3$  (blue squares),  $2048^3$  (green diamonds), and  $4096^3$  (red circles).

703 the new bound’s curve is comparable to the slope of the  
 704 vorticity-supremum-norm curve.

705 In order to make a more quantitative comparison of the  
 706 slopes, Fig. 6(b) shows the logarithmic rates of growth for  
 707 old bound, new bound, and vorticity supremum norm. In that  
 708 order, these rates satisfy the ratios 7 : 5 : 4 at the resolved time  
 709  $t \approx 3.85$ .

710 **B. Analysis of  $\delta$  in terms of BKM**

711 We now proceed to see if the accelerated decay observed in  
 712 the decrement  $\delta(t)$  and quantified in Fig. 4(d) can correspond  
 713 to a power law. To wit, we use the same local three-point  
 714 method as that described in Sec. III C [see Eqs. (9)–(11)]. The  
 715 behavior of  $g(t)$  is presented in Fig. 7 and the corresponding  
 716  $T_*(t)$  and  $\Gamma(t)$  are presented in Table IV.

717 The results for the exponent and predicted singular time of  
 718 Table IV have to be read carefully. Because of the local three-  
 719 point method used to derive them from the data in Table II, they  
 720 use the values of  $\delta$  at  $t = 3.65, 3.7, 3.75, 3.8, 3.85$ , the last one  
 721 being marginally reliable (see Sec. III B). In fact, they amount  
 722 to a linear two-point extrapolation of the data in Fig. 7 (see  
 723 the inset):  $T_*$  is the intersection of the straight line extrapolation  
 724 with the time axis and  $\Gamma$  is the inverse of the slope. One can  
 725 guess that there is room for a power-law type of behavior, with  
 726 exponent  $\Gamma \approx 0.4$  if we consider the data at  $t = 3.7, 3.75$  and  
 727  $\Gamma \approx 1.4$  if we include the data at  $t = 3.8$ .

TABLE IV. Power-law fit parameters  $\Gamma$  and  $T_*$  [see Eq. (8)] for  $\delta(t)$  determined at resolution  $4096^3$  on full interval  $3 < k < k_{\max}$  (same as in Figs. 4 and 7) and on subinterval  $103 < k < k_{\max}$  (see Table II).

Time	$\Gamma$	$\Gamma$	$T_*$	$T_*$
	$3 - k_{\max}$	$103 - k_{\max}$	$3 - k_{\max}$	$103 - k_{\max}$
3.7	0.283	0.383	3.81	3.83
3.75	0.354	0.393	3.83	3.83
3.8	1.41	1.36	4.00	3.97

We now use Corollary 11 (see Sec. IV) to test if these estimates of the power law are consistent with the hypothesis of finite-time singularity. There, the product  $\Gamma(6 - n_-)/2$  must be greater than or equal to 1 if finite-time singularity is to be expected. With the conservative estimate  $n_- = 3.9$  obtained by inspection of Fig. 4(b) (or equivalently using the values of  $n$  in Table II), we obtain that  $\Gamma(6 - n_-)/2 < 1$  for the data at  $t = 3.7$  and  $3.75$ , but  $\Gamma(6 - n_-)/2 > 1$  for the data at  $t = 3.8$ . These results are insensitive to the fit interval; see Table IV. Therefore, if the latest data are considered, Corollary 11 cannot be used to negate the validity of the hypothesis of finite-time singularity. However, there is no sign that the data values of  $\Gamma$  and  $T_*$  in Table IV are settling down into constants, corresponding to a simple power-law behavior.

Another piece of analysis consists of comparing the singular time predicted from the data for the decrement  $\delta(t)$  with the singular time predicted from the direct data for the vorticity supremum norm. They seem both to be close to  $T_* \approx 4$  (compare Tables IV and III).

In this context, we should perhaps mention Feynman’s rule, “Never trust the data point furthest to the right,” a comment attributed to Richard Feynman, saying basically that he would never trust the last points on an experimental graph, because if the people taking data could have gone beyond that, they would have. Higher-resolution simulations are clearly needed to investigate whether the new regime is genuinely a power law and not simply a crossover to a faster exponential decay.

Our conclusion for this section is thus similar to that of Sec. III C: although our late-time reliable data for  $\delta(t)$  show  $\Gamma(6 - n_-)/2 > 1$  and are therefore not inconsistent with our Corollary 11, clear power-law behavior of  $\delta(t)$  is not achieved.

## VI. CONCLUSIONS

In summary, we presented simulations of the Taylor-Green vortex with resolutions up to  $4096^3$ . We used the analyticity-strip method to analyze the energy spectrum. We found that, around  $t \simeq 3.7$ , a (well-resolved up to  $t \simeq 3.85$ ) change of regime takes place, leading to a faster decay of the width of the analyticity strip  $\delta(t)$ . In the same time interval, preliminary 3D visualizations displayed a collision of vortex sheets. Applying the BKM criterion to the growth of the maximum of the vorticity on the time interval  $3.7 < t < 3.85$ , we found that the occurrence of a singularity around  $t \simeq 4$  was not ruled out but that higher-resolution simulations were needed to confirm a clear power-law behavior for  $\|\omega\|_\infty(t)$ .

We introduced a new sharp bound for the supremum norm of the vorticity in terms of the energy spectrum. This bound allowed us to combine the BKM theorem with the analyticity-strip method and to show that a finite-time blowup can exist only if  $\delta(t)$  vanishes sufficiently fast. Applying this new test to our highest-resolution numerical simulation we found that the behavior of  $\delta(t)$  is not inconsistent with a singularity. However, due to the rather short time interval on which  $\delta(t)$  is both well resolved and behaving as a power law, higher-resolution studies are needed to investigate whether the new regime is genuinely a power law and not simply a crossover to a faster exponential decay.

Let us finally remark that our formal assumptions of Sec. IV C are motivated and to some extent justified by the

fact that, in systems that are known to lead to finite-time singularity, the equivalent of the working hypothesis Eq. (17) is verified. For the analogy to apply, a version of the BKM theorem must be available. This is the case of the 1D inviscid Burgers equation for a real scalar field  $u(x, t)$  defined on the torus:

$$\frac{\partial u}{\partial t} + u \frac{\partial u}{\partial x} = 0 \quad \forall x \in [0, 2\pi], \quad \forall t \in [0, T_*),$$

which admits a BKM type of theorem [25], with singularity time  $T_*$  defined by  $\int^{T_*} \|u_x(\cdot, t)\|_\infty dt = \infty$ .

In the 1D case, the equivalent of our bound Eq. (21) is

$$\|u_x(\cdot, t)\|_\infty \leq \tilde{c} \sum_{k=1}^{\infty} k \sqrt{E(k, t)}.$$

Using the simple trigonometric initial data  $u(x, 0) = \sin(x)$ , the energy spectrum can be expressed in terms of Bessel functions that admit simple asymptotic expansions. It is straightforward to show (see [10] for details) that, for  $t < T_* = 1$ , one has the large- $k$  asymptotic expansion

$$E(k, t) \sim \frac{1}{\pi t^2 \sqrt{1-t^2}} k^{-3} e^{-2\delta_S(t)k},$$

with

$$\delta_S(t) = \ln \left( \frac{\sqrt{1-t^2} + 1}{t} \right) - \sqrt{1-t^2},$$

while, at  $t = T_* = 1$ ,

$$E(k, 1) \sim \frac{2 \cdot 6^{2/3}}{\Gamma(-\frac{1}{3})^2} k^{-8/3}.$$

In fact, the  $k^{-8/3}$  power law appears already before  $T_*$  [see the remark following Eqs. (3)–(10) of [10]].

It is easy to check that the analytical solution admits, for all  $k$  and for all  $t$  sufficiently close to  $T_*$ , a working hypothesis Eq. (17) of the form

$$E(k, t) \leq M k^{-n_0} \exp(-2 \delta_0(t) k),$$

with analytically obtainable functions  $n_0(t) = 8/3$  and  $\delta_0(t) \propto (T_* - t)^\Gamma$  with  $\Gamma = 3/2$ . The equivalent of Corollary 11 gives the inequality

$$\Gamma \geq \frac{2}{4 - n_0},$$

which is saturated by the analytically obtained exponents  $n_0 = 8/3$ ,  $\Gamma = 3/2$ .

## ACKNOWLEDGMENTS

We acknowledge useful scientific discussions with Annick Pouquet, Uriel Frisch, and Giorgio Krstulovic, who also helped us with the visualizations of Fig. 2. The computations were carried out at Institut du Développement et des Ressources en Informatique Scientifique (CNRS). Support for this work was provided by University College Dublin Seed Funding Projects No. SF304 and No. SF564 and the Irish Research Council for Science, Engineering, and Technology Ulysses project “Singularities in three-dimensional Euler equations: simulations and geometry.”

823 **APPENDIX: EXTENSION TO GENERAL**  
824 **PERIODIC FLOWS**

825 Here we provide the generalization to non-TG-symmetric  
826 periodic flows of the results presented in Sec. IV C.  
827 Definition 2 and the working hypothesis (Hypothesis 3) are  
828 modified slightly in the general case. Accordingly, the new  
829 bounds leading to Lemma 7 and Theorem 8 need to be modified  
830 slightly to accommodate the general case. The crucial derived  
831 relations between  $\delta_0$  and  $n_0$  in Lemma 6 and Corollaries 10  
832 and 11 will apply directly to the general periodic case and will  
833 not be discussed.

834 The main technical difference is that the new bounds  
835 presented in Sec. IV C apply for a flow with TG symmetries  
836 (see Sec. II B) which imply that only modes with even-  
837 even-even and odd-odd-odd wave-number components are  
838 populated. The general periodic case does not follow this  
839 restriction, which slightly modifies the bounds. We will  
840 assume, to simplify matters, that the so-called zero mode of  
841 the velocity field is identically zero:

$$\hat{\mathbf{u}}(\mathbf{0}, t) = \mathbf{0}, \quad \forall t \in [0, T).$$

842 Notice that all remaining wave numbers are populated. This  
843 means that all sums involving the scalar  $k$  in Eqs. (18) and (21)  
844 will start effectively from  $k = 1$ .

845 Also, because modes with mixed even-odd wave-  
846 number components are allowed, the definitions of  $S_k$  in  
847 Lemma 2 and constant  $c$  in Eq. (21) must be replaced by more  
848 appropriate quantities. Therefore, the corresponding general  
849 periodic versions of Lemma 7 [Eq. (18)] and the practical  
850 bound [Eq. (21)] are the following:

*Lemma 7' (general periodic version of Lemma 7).* Let  $\mathbf{u}(\mathbf{x}, t)$  be a velocity field with energy spectrum defined by Eq. (4) and let  $\omega = \nabla \times \mathbf{u}$  be its vorticity, defined on the periodicity domain  $D = [0, 2\pi]^3$ . Then the following inequality is verified for all times  $t \in [0, T)$  when the sum in the right-hand side is defined, and independently of any evolution equation that  $\mathbf{u}$  might satisfy:

$$\|\omega(\cdot, t)\|_\infty \leq \sum_{k=1}^{\infty} \sqrt{2k(k+1)E(k, t)S'_k}, \quad (\text{A1})$$

where  $S'_k \equiv \#\{\mathbf{k} \in \mathbb{Z}^3 : k - 1/2 < |\mathbf{k}| < k + 1/2\}$  is the number of lattice points in a spherical shell of width 1 and radius  $k \in \mathbb{Z}_+$ .

*Practical bound, general case.*

$$\|\omega(\cdot, t)\|_\infty \leq c' \sum_{k=1}^{\infty} k^2 \sqrt{E(k, t)}, \quad (\text{A2})$$

where  $c' = 6\sqrt{2}$ .

We can easily check that the bounds for Taylor-Green, Eqs. (18) and (21), are sharper (by a factor close to 2) to their respective general bounds, Eqs. (A1) and (A2).

Finally, Theorem 8 is replaced by the following:

*Theorem 8'.* Let a solution of the 3D Euler equations satisfy the working hypothesis Eq. (17) with  $k = 1$  included. Then the maximal regularity time  $T_*$  of the solution must satisfy

$$\int_0^{T_*} \text{Li} \left( \frac{n_0(t)}{2} - 2e^{-\delta_0(t)} \right) dt = \infty.$$

- 
- [1] J. T. Beale, T. Kato, and A. Majda, *Commun. Math. Phys.* **94**, 61 (1984).  
 [2] C. Bardos and E. Titi, *Russian Mathematical Surveys* **62**, 409 (2007).  
 [3] R. Kerr, *Phys. Fluids* **17**, 075103 (2005).  
 [4] T. Y. Hou and R. Li, *J. Nonlinear Sci.* **16**, 639 (2006).  
 [5] M. D. Bustamante and R. M. Kerr, *Physica D: Nonlinear Phenom.* **237**, 1912 (2008).  
 [6] J. Gibbon, *Physica D: Nonlinear Phenom.* **237**, 1894 (2008).  
 [7] P. Constantin, C. Fefferman, and A. J. Majda, *Communications in Partial Differential Equations* **21**, 559 (1996).  
 [8] J. Deng, T. Y. Hou, and X. Yu, *Communications in Partial Differential Equations* **30**, 225 (2005).  
 [9] J. Deng, T. Y. Hou, and X. Yu, *Communications in Partial Differential Equations* **31**, 293 (2006).  
 [10] C. Sulem, P.-L. Sulem, and H. Frisch, *J. Comput. Phys.* **50**, 138 (1983).  
 [11] C. Bardos and S. Benachour, *Annali della Scuola Normale Superiore di Pisa, Classe di Scienze, Sér. 4* **4**, 647 (1977).  
 [12] D. Gottlieb and S. A. Orszag, *Numerical Analysis of Spectral Methods* (SIAM, Philadelphia, 1977).  
 [13] U. Frisch, *Turbulence: The Legacy of A. N. Kolmogorov* (Cambridge University Press, Cambridge, 1995).  
 [14] U. Frisch, T. Matsumoto, and J. Bec, *J. Stat. Phys.* **113**, 761 (2003).  
 [15] G. I. Taylor and A. E. Green, *Proc. R. Soc. A* **158**, 499 (1937).  
 [16] M. E. Brachet, D. I. Meiron, S. A. Orszag, B. G. Nickel, R. H. Morf, and U. Frisch, *J. Fluid Mech.* **130** (1983).  
 [17] M. E. Brachet, M. Meneguzzi, A. Vincent, H. Politano, and P. L. Sulem, *Phys. Fluids A* **4**, 2845 (1992).  
 [18] C. Cichowlas and M.-E. Brachet, *Fluid Dyn. Res.* **36**, 239 (2005).  
 [19] E. Lee, M. E. Brachet, A. Pouquet, P. D. Mininni, and D. Rosenberg, *Phys. Rev. E* **78**, 066401 (2008).  
 [20] A. Pouquet, E. Lee, M. E. Brachet, P. D. Mininni, and D. Rosenberg, *Geophys. Astrophys. Fluid Dyn.* **104**, 115 (2010).  
 [21] P. D. Mininni, D. Rosenberg, R. Reddy, and A. Pouquet, *Parallel Computing* **37**, 316 (2011).  
 [22] S. S. Ray (private communication).  
 [23] S. S. Ray, U. Frisch, S. Nazarenko, and T. Matsumoto, *Phys. Rev. E* **84**, 016301 (2011).  
 [24] I. Kukavica and V. C. Vicol, *Discrete and Continuous Dynamical Systems A* **29**, 285 (2011).  
 [25] M. D. Bustamante, *Physica D: Nonlinear Phenom.* **240**, 1092 (2011).